Changes of water/ice morphological, thermodynamic, and mechanical parameters during the freezing process

Qian Cong[a, b], Jin Xu[a], Luquan Ren[a, c], Jingfu Jin[c], Tingkun Chen[a, c, *], Kwang Leong Choy[d]

[a] Key Laboratory of Bionic Engineering, Ministry of Education, Jilin University, Changchun 130022, P. R. China.

[b] State Key Laboratory of Automotive Simulation and Control, Jilin University, Changchun 130022, P. R. China.

[c] College of Biological and Agricultural Engineering, Jilin University, Changchun 130022, P. R. China.

[d] Institute for Materials Discovery, University College London, London WC1E 7JE, United Kingdom.

ABSTRACT

To reduce ice adhesion hazards, optimize or develop the anti/de-icing methods, it is necessary to understand the change of freezing parameters during the freezing process, such as thermodynamic, morphological, and mechanical parameters. The present study investigates the freezing characteristics by purposely–built devices to describe the freezing process quantitatively. Morphological parameters were calculated the reverse engineering. The results showed that the inner temperature and morphology of water droplet were obviously changed, and the freezing process could be mainly divided into three stages: initial and spreading, freezing, and steady-state.

*Corresponding authors at: Jilin University, No. 5988 Renmin Street, Changchun 130022, P. R. China.

E–mail address: chentk@jlu.edu.cn (T K. Chen)

Fax: +86–431–85095575–888

Moreover, an experimental apparatus that measured the phase swelling force was built on investigating the freezing process of water from the mechanical aspect. It was found that the swelling force generated from the freezing process of 2473 mm^3 water could reach 46.38 N. The generation process of swelling force could also be separated into three stages: non–expansive stage, increasing stage, and stable stage. The formation stage of swelling force was similar to that of ice. Combining the measured expansion force with the calculated freezing parameters based on the observed test, the freezing process of water could be better understood. The study would help researchers and engineers understand the freezing process and provide some freezing characteristics parameters for the anti/de-icing research.

Keywords: Freezing process; Freezing characteristics parameters; Morphology; Thermodynamics; Mechanics.

1. Introduction

In cold–climate regions, water in the environment, such as moisture and rain, inevitably accumulates on the exposed components and freezes into ice. This is a common occurrence that not only causes an increasing load of parts but also leads to changing the surface characteristics of the components, such as topography, wetting, light transmittance, and other surface properties [1-3]. These issues caused by ice accreted have affected many industrial areas. For example, the aerodynamic performance and dynamic balance of the wind blade will be altered by the surface morphology owing to ice adhesion, and the productivity and safety of the wind blade

will also be reduced [4-8]. Moreover, the accreted ice has affected other engineering fields and caused many hazards, such as solar panel covered by ice reducing the photoelectric conversion efficiency, and affecting the operation safety of the high-speed train, and increase the load of transmission line and resulting in the cable to break [9-15].

To diminish the influence of ice adhesion, researchers and engineers have developed more than 30 kinds of anti/de-icing methods. According to the anti/de-icing principles, these conventional technologies can be classified into three categories: mechanical ways to remove accreted ice directly, heating methods to melt the covered ice or delay freezing, and chemical methods to change the phase temperature of water to delay freezing [16-19]. Although these technologies have an excellent anti/de-icing effect, there are some disadvantages during the actual use, such as high cost, high energy consumption, and environmental pollution [20-25]. So, a new anti/de-icing method is urgently needed in engineering. With the discovery of the lotus leaf phenomenon and the recent developments in materials fabrication, the surface wettability is changed by the surface-modified technology to make it with the hydrophobic property. Superhydrophobic surfaces are a promising method to prevent ice accreted on exposed surfaces due to their remarkable water-repellency. However, several studies have shown that superhydrophobic surfaces have some limitations, such as the poor durability of their anti/de-icing effect and poor mechanical stability [25-34]. Kulinich et al. [35] and Farhadi et al. [36] found that the wettability of the superhydrophobic surface was gradually lost owing to the destruction of the

microstructure after several anti/de-icing cycles. So, the practical application of such surfaces should maintain their properties to meet the actual use requirements.

In order to develop or optimize the anti/de-icing technology, the freezing process of water droplets and the various freezing parameters should be better understood. For example, the swelling force generated from the freezing process can be used as the active anti/de-icing power to develop a new anti/de-icing technology [37-38]. Meanwhile, the study of the freezing process and its characteristic parameters can provide a reference for simulation in some engineering fields, such as the simulation of ice formation on the surface of aircraft wings and wind blades.

However, observing the freezing process of water droplets on the cold surface is usually to verify the anti/de-icing effect of the newly developed technology or newly fabricated surface [39-41]. Hence, this work observes the freezing process of water droplets on the cold surface by the self-made device. And the freezing characteristic parameters, such as morphological, thermodynamic, and mechanical properties, were collected to characterize the freezing process. The morphology was described by the shape and size of water/ice during the freezing process, and the internal temperature indicates the thermodynamics. The swelling force generated by the phase change could be measured by a purposely–built apparatus to represent the mechanical properties of the freezing process. This research will be helpful to analyze ice adhesion mechanisms using finite element simulation methods in aviation, wind turbines, and other engineering fields. It will also lay a foundation for developing new anti-icing methods and optimizing the existing conventional anti/de-icing methods.

2. Materials and methods

The present study took the research approach shown in Fig. 1 to study the changes of parameters during the freezing process.

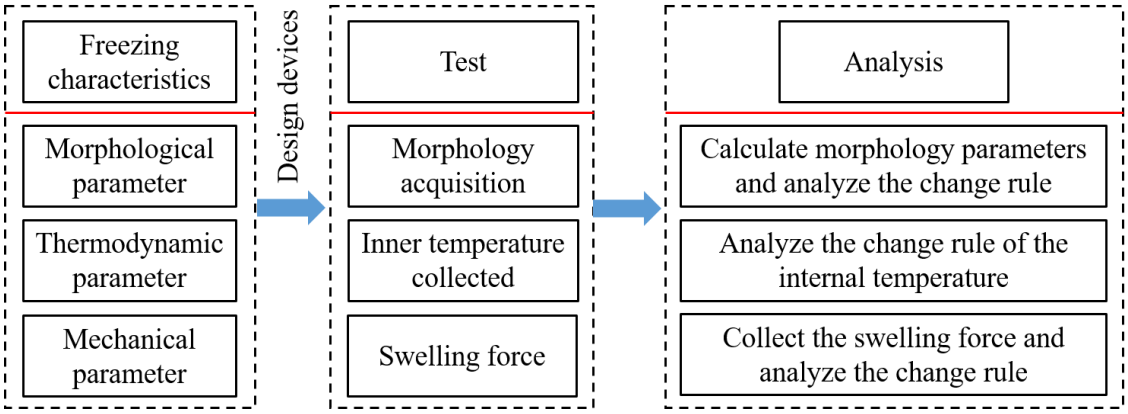

Fig.1 Schematic of the research approach.

2.1 Materials

During the test, 6061 aluminum alloy and copper plates were purchased from the Haerbin Dongbeilong Metal Co., Ltd., Heilongjiang (China) as the sample material. Pure water, acetone (Tianjin East China Chemicals Co. Ltd.) in the study were used for ice preparation and material cleaning.

2.2 Experimental apparatuses

The purposely built apparatus was to observe the freezing process and collect the characteristic parameters due to the lack of a commercial device.

2.2.1 Morphology acquisition device

Water not only spreads on the cold surfaces but also changes its appearance and shape during the ice formation process until it reaches a stable state. However, the

existing research only observed the freezing process of water on the material surface and its shape from the horizontal or vertical direction. A multidimensional microscopic observation device shown in Fig. 2, was set up in this study to understand the freezing process of the water droplet on the cold surface from different dimensions, and the dynamic changes in the shape of water or ice were changed.

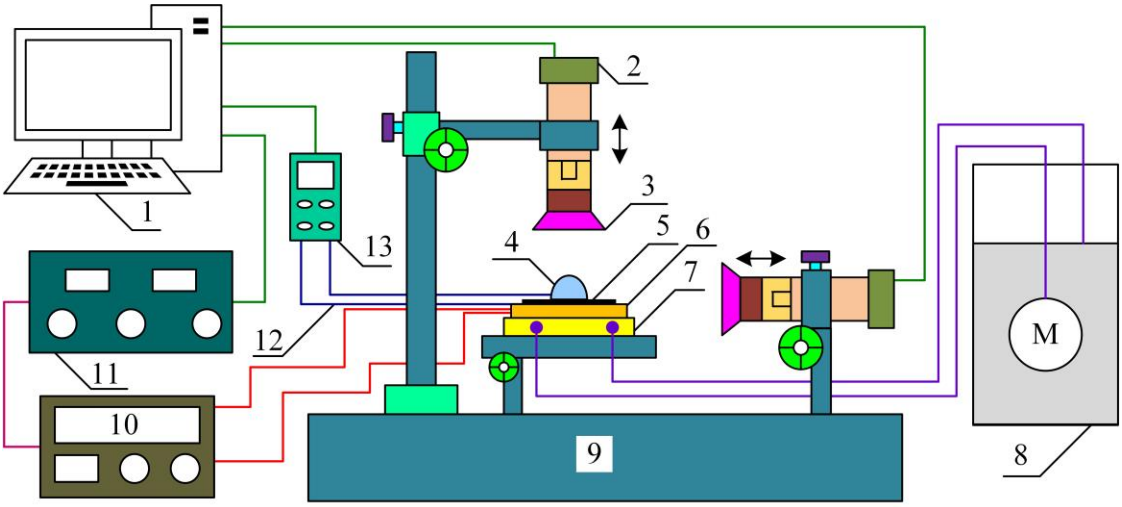

Fig.2 Schematic illustration of the morphology acquisition device.

1. PC; 2. CCD camera; 3. Microscope; 4. Water droplet; 5. Sample; 6. Semiconductor refrigeration unit; 7. Refrigeration stage; 8. Cooled bath; 9. Bench; 10. DC Power; 11. Temperature controller; 12. K–type thermocouple; 13. Multichannel temperature recorder.

As shown in Fig. 2, the observation device consisted of two microscopes, an image collection system, a cooling bath, K–type thermocouples, data acquisition, DC power, and a refrigeration system based on the Peltier effect. By adjusting the voltage of the DC power supply connected with the semiconductor-based on the Peltier effect, the sample would be refrigerated to the set temperature. During the freezing process, the ambient temperature, the surface temperature of the sample, and the internal

temperature of droplet or ice were simultaneously measured K–type thermocouples and transmitted to the multichannel temperature recorder. The accuracy of the thermocouple was ±1.0%. The ice formation process was synchronously recorded by two microscopes (with the CCD camera) placed horizontally and vertically. The image sequence was recorded in the computer by the data acquisition system, and the time interval between the two images was one second.

2.2.2 Swelling force test device

It is well known that water attached to the material surface will phase change during the freezing process. The swelling force generated from the phase change process will act on the constraint boundary, such as the bursting of aluminum water tanks in the winter. However, the swelling force regarded as one of the important parameters during the freezing process was always neglected. The purposely–built apparatus was designed to evaluate the swelling force generated during the ice formation process based on the action and reaction principle. As shown in Fig. 3, the device was composed of the draft gauge, an aluminum alloy plate with a pit, a screw pair, and other components. The hole of the aluminum alloy plate was used as a container for water.

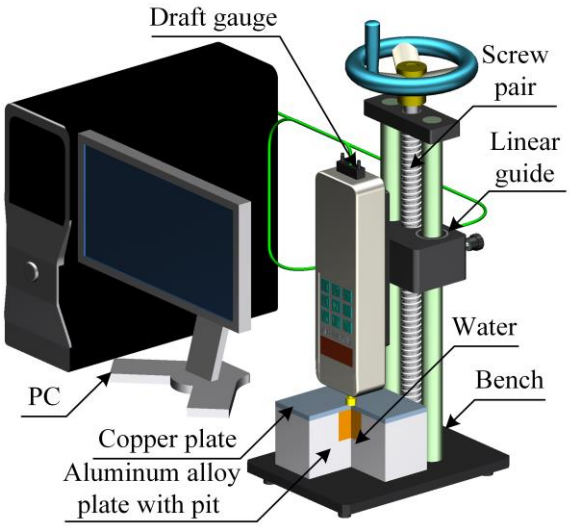

Fig.3 Swelling force test device.

In order to accurately measure the swelling force generated by freezing water in the pit and reduce the deformation of the container wall caused by the frost-heaving force, the thickness of the vessel wall and the size of the pit were increased. The Al-alloy plate ($100 \times 100 \times 30$ mm^3 in size) had a pit with a diameter of 30 mm and a depth of 3.5 mm, which was formed in the central area of the plate and was filled with water. A copper plate covered the pit. The water close to the copper plater would freeze first at a low-temperature due to the difference in thermal conductivity between aluminum alloy and copper. And this would avoid the overflow of water close to the copper plate due to the expansion of the water in the bottom. The draft gauge with a force sensor was used to inspect the swelling force dynamically, and the force was simultaneously transmitted to a computer. The push-pull mechanism was limited by the clamping bolt on the linear guide. The measurement precision of the draft gauge was ± 0.01 N.

2.3 Experimental procedures

2.3.1 Morphology acquisition tests

Before the test, the Al-alloy surface was cleaned with acetone, and the substrate was adhered to the semiconductor refrigeration unit with thermally conductive grease to fill the microscopic air–gap between the two surfaces. Then the DC power voltage was adjusted, and the surface temperature of the sample reached the set temperature. In this study, the surface temperature of the Al-alloy was set to –10 ℃. Until the surface temperature of the substrate was stable, five microliters of water were carefully dropped onto the sample surface using a micropipette. Two microscopes in the observation device were adjusted to focus on the water droplet located on the sample surface. After the test, the Al-alloy surface was cleaned in an acetone ultrasonic bath for 5 min and in a deionized water ultrasonic bath for another 5 min. The samples were then dried in an oven at 60 ℃.

The freezing process of the water droplets on the material surface was dynamically recorded by the device shown in Fig. 2, and the temperature during the freezing process was collected. The freezing characteristic parameters shown in Fig. 4 were measured and calculated by reverse engineering.

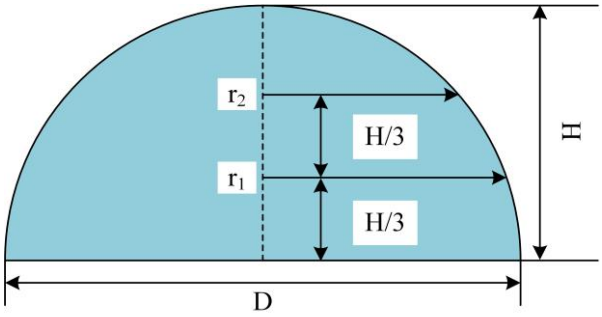

Fig.4 Freezing characteristic parameters during the freezing process.

2.3.2 Swelling force tests

Because of the large volume of the pit in the swelling force measurement experiment, the ambient temperature was set to -25 ℃. The water near the copper plate would first freeze into ice due to the difference between the pit boundary and thickness of the copper plate as well as the thermal conductivity of the two, and the pit was axisymmetric. Hence, the force measured by the device could be regarded as the swelling force generated by the water in the pit.

During the experiments, the entire device was placed in a climate chamber controlled to an ambient temperature of –25 ℃. The draft gauge was aligned with the center area of the copper plate with a pit. The swelling force generated by water in the pit would directly act on the copper plate, and the force was synchronously transmitted to the PC. The time interval between two acquisition forces was one millisecond.

3. Results

3.1 Morphological parameters

3.1.1 Morphology of water/ice on the material surface

The morphology of water droplets on the cold surface was collected by the horizontal and vertical microscopes, as shown in Fig. 5. When viewed from the vertical direction, the contact length l_1, l_2, L_1, *and* L_2 between the water droplet or ice and Al-alloy surface before and after freezing were calculated using the scale method. The contact lengths L_2 and L_1 were approximately l_2 and 0.99 times of l_1, respectively.

It could be concluded that the shape of the droplet adhering to the cold surface was regarded as a circular shape from a vertical direction view.

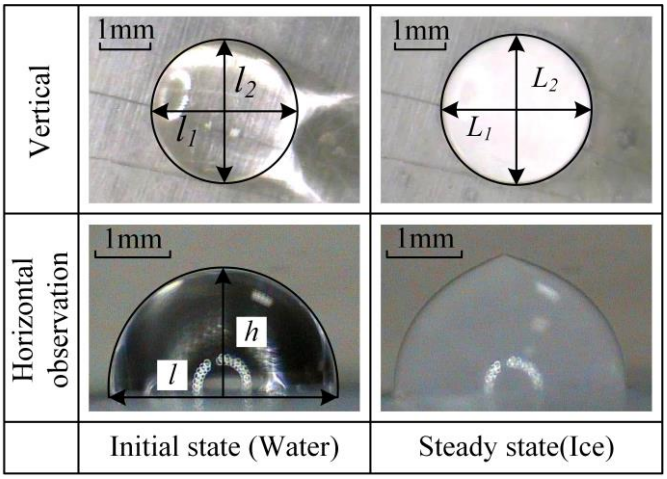

Fig.5 Morphology of water droplet in different directions on the cold surface.

The same method was used to analyze the relationship between the height of the droplet on the cold surface and the contact length in the initial state. It could be seen that the shape of the water droplets on the surface of the sample was an approximately semicircular shape when viewed from the horizontal direction. Therefore, the shape of the water droplet on the sample surface could be regarded as the hemispherical shape (in agreement with [39, 42-44]), and the morphological parameters of water or ice on the sample surface could be calculated according to a hemisphere.

3.1.2 Calculation of the morphological parameters

The titration time of water droplets was used as the initial time for morphological capture. The characteristic morphological parameters shown in Fig. 4 were calculated by using the tracing point method. This method has been validated by several studies [42-47]. So the calculation results of morphological parameters were shown in Fig. 6.

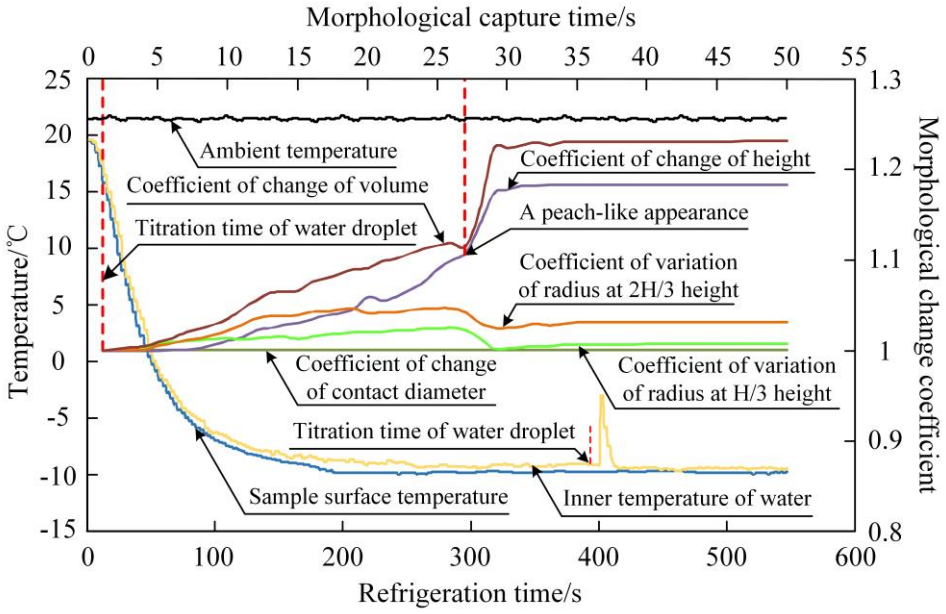

Fig.6 Morphological parameters and Temperatures.

As shown in Fig. 6, the water droplet rapidly phased and frozen when the water droplet was placed on the Al-alloy surface. After the water droplet was titrated on the Al-alloy surface at –10 ℃ for about 50 seconds, the morphology of the ice on the material surface reached a stable state. The contact length between the water droplet and the material did not change significantly. The cross-section had a different interface radius to varying heights of the water droplet or ice. And the radius of the cross-sectional at 2/3 and 1/3 of the initial height of the droplet had the same change trend. This meant that the cross-sectional diameter gradually increased with the continuous cooling and then decreased, and finally tended to be stable. Moreover, the change in radius at different locations also indicated that water was hemispherical on the material surface. As the cooling continued, water height and volume gradually increased, rapidly rose to the maximum value, and stabilized. As shown in Fig. 6, the height direction was the mainly expansive direction. And the change in height was

more obvious than the difference in the section diameter at different heights of the water or ice.

3.2 Mechanical parameters

The swelling force generated by the water in the pit was measured, as shown by curve 1 in Fig. 7. Additionally, the inner temperature of the water in the pit during the freezing process was collected, as shown by curve 2 in Fig. 7. The swelling force generated by the water in the pit with a diameter of 30 mm and a depth of 3.5 mm could reach 46.38 N in a short time.

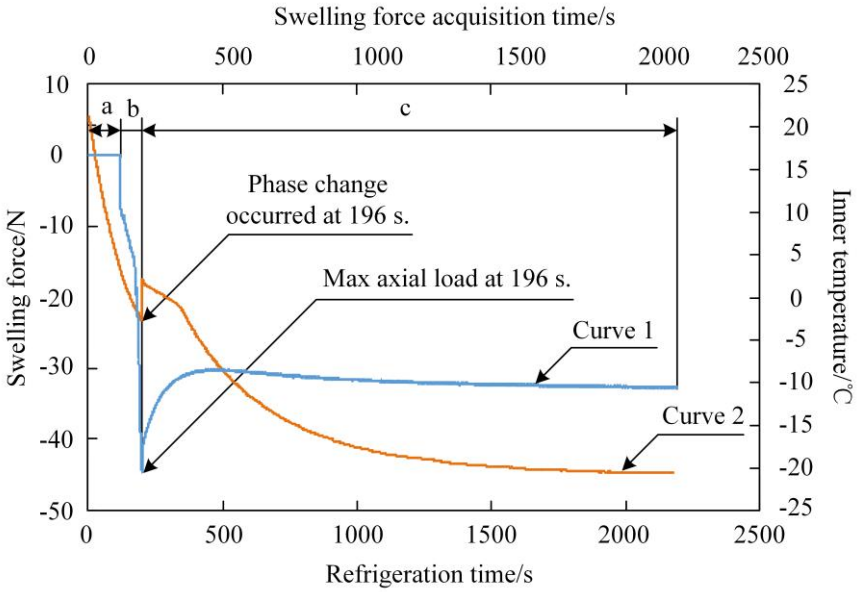

Fig.7 The curve of temperature and swelling force during the freezing process.

In combination with curves 1 and 2 in Fig. 7, the internal temperature of the water in the pit gradually decreased under the low-temperature environment, and the swelling force was not generated due to the water entering into a supercooled state. Then the swelling force was generated from the water in the pit and increased rapidly, and the inner temperature of the water filling the pit began to change. When the

swelling force reached the maximum value, it rapidly decreased and reached a steady state. Additionally, the internal temperature of the water filling in the pit had reached the same state. In summary, the phase change process could be divided into three stages depending on the generation process of the swelling force: no-load, frost–heaving force increased, then the force tended to be stable.

3.3 Thermodynamic parameters

Meanwhile, the temperature during the ice formation process was also collected, as shown in Fig. 6. When the water droplet was titrated on the cold surface, the phase change occurred rapidly, and the water droplet frozen into ice. It could be seen from Fig. 6 and Fig. 7 that no matter whether the ambient temperature was –10 ℃ or –25 ℃, the internal temperature of the water would suddenly increase during the freezing process, accompanied by the significant changes in the morphology and mechanical properties. Due to the difference in substrate thickness and water volume, there was a significant difference in freezing time between the morphology observation test and the swelling force measurement test.

As shown in Fig. 7, the change process of the inner temperature of the water filling in the pit was similar to the b and c stages of the swelling force. The internal temperature change process could be separated into four distinct periods: the decrease, suddenly rising, then falling, and the reaching stability periods.

4. Discussion

Regardless of the surface temperature, the water attached to the substrate surface

had the same process, except that the occurrence time and duration of each stage was different. So, in order to understand the freezing characteristic parameters, the freezing process of the water on the surface at –10 ℃ was observed, as shown in Fig. 8. When the water droplet was titrated on the substrate surface, the surface with low temperature formed an anchoring effect on the water attached to the material surface, which limited the spread of water on the material surface. The contact length between water and material did not change obviously, and the freezing front appeared in the water droplet.

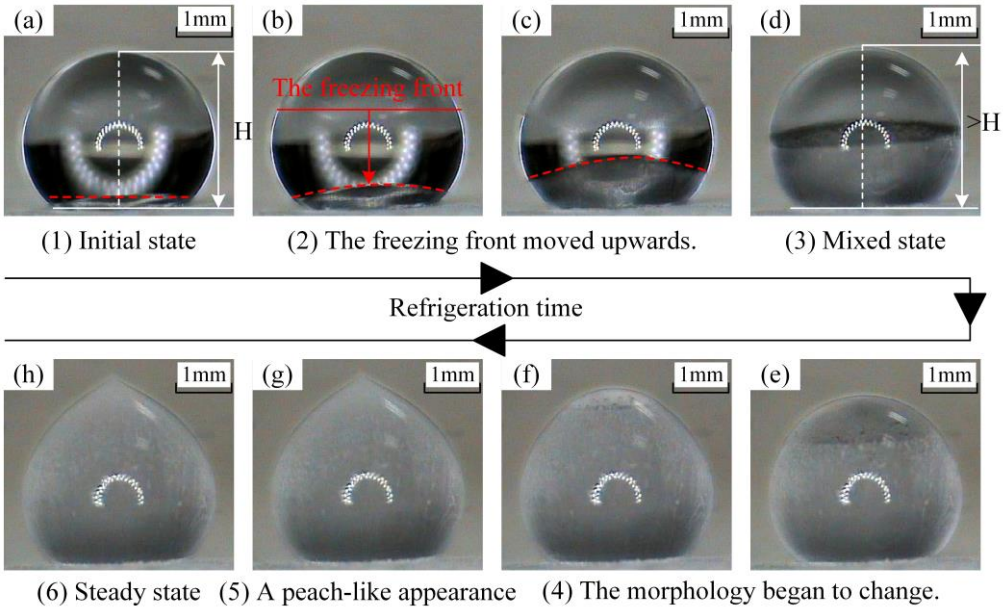

Fig.8 The microscopic observation of the freezing process of the water droplet on the Al-alloy surface.

As the freezing front moved from the bottom to the top of the water droplet, the droplet became muddy and lost its transparency, as shown in Fig. 8. The mixture of water and ice was formed between the frozen front and the Al-alloy surface (images a-d of Fig. 8). It meant that the combination entered into the supercooled state. The cross-section diameter at different heights would increase under the action of the

hemispherical shape and the gravity of the water droplet on the cold surface. The mixture under the freezing front would form an anchoring effect on the supercooled water above the freezing front, which would limit the increase in the cross-sectional diameter at different heights. Additionally, the surface tension of water was not conducive to the rise of the diameter. It could be seen from Fig. 8 (images a-f) that the height of the water droplet had changed significantly relative to the initial state. When the phase change finished, the hemispherical water droplet on the Al-alloy surface became into the ice with a peach-like shape, and the height of the water or ice reached the maximum value. After the ice formed on the substrate surface reached a stable state, its morphological parameters did not change significantly.

During the swelling force measurement experiment, the wall thickness of the pit and the volume of the water were more massive than the size of the Al-alloy plate and the volume of water used in the morphology observation test. Therefore, compared with the freezing time in the observation test, the water in the pit would be in the supercooled state for a longer time. When the water filling in the pit began to phase change, the swelling force started to increase. It could be seen from Fig. 6 that the expansive direction of the water droplet on the Al-alloy surface was mainly the height direction. The height of water increased rapidly when it began to freeze. So, the frost-heaving force generated by the water filling in the pit also increased rapidly, as shown in Fig. 7. When the water in the pit phased into ice, the swelling force reached the maximum value, 46.38 N. Meanwhile, the draft gauge exerted a reaction force on the copper plate owing to the reaction and reaction. This might reduce the swelling

force. When the swelling force generated by the water filling in the pit was equal to the pressure exerted by the draft gauge on the copper plate, the swelling force was inclined to be stable.

5. Conclusions

The morphology of water on the Al-alloy surface was observed from different directions by a purposely-built apparatus, and the internal temperature of the water droplet was collected during the process. The morphological parameters during the freezing process were measured and calculated by the tracing method. Meanwhile, another important parameter during the freezing process of water, namely the swelling force, was measured by the purposely-built device. The swelling force generated by water in the pit could reach 46.38 N in a short time.

It could be seen from the experimental results that the freezing characteristic parameters, including the morphology, thermodynamics, and mechanics, had a similar process. The morphology of water on the substrate surface could be regarded as a hemispherical shape based on the morphological observation test and the calculated parameter. When water was dropped onto the Al-alloy surface, the cold surface would limit the water spread on the substrate surface. After the freezing front appeared, it moved from bottom to top, and the area after moving decreased the transparency gradually. Due to the hemispherical shape of the water on the substrate surface and under the action of gravity, the cross-section diameter at different heights increased during the freezing process. The height of water or ice on the Al-alloy surface also

gradually increased. According to the experiment results, the main expansion direction of water on the sample surface was height, about 1.18 times of the initial state. The swelling force gradually increased with the increase in height. When the water was completely frozen into ice, the height reached the maximum value, accompanied by the swelling force generated by water filling in the pit, getting the maximum value.

In conclusion, the purposely-built devices were used to measure and collect the morphology, thermodynamic, and mechanical parameters during the freezing process. The test results may help researchers optimize the existing anti/de-icing methods and develop new anti/de-icing technology. The present work will help provide an experimental basis for mathematical modeling of the freezing process, so the influence of ice adhesion on some engineering fields may be analyzed.

Acknowledgments

This work was supported by the National Natural Science Foundation of China (Grant No. 51775234), the Department of Science and Technology of Jilin Province, China (Grant No. 20200801049GH), and the State Key Laboratory of Automotive Simulation and Control (Grant No. 20171115).

References

1. Corradini, M.L.; Ippoliti, G.; Orlando, G.: A sliding mode observer–based icing detection and estimation scheme for wind turbines. J. Dyn. Syst. Meas. Control-Trans. ASME. **140**(1), no014502 (2018)

2. Jelle, B.P.: The challenge of removing snow downfall on photovoltaic solar cell roofs in order to maximize solar energy efficiency–Research opportunities for the future. Energy and Build. **67**, 334–351 (2013)
3. Pérez, J.M.P.; Márquez, F.P.G.; Hernández, D.R.: Economic viability analysis for icing blades detection in wind turbines. J. Clean. Prod. **135**, 1150–1160 (2016)
4. Hu, L.Q.; Zhu, X.C.; Hu, C.X.; Chen, J.G.; Du, Z.H.: Wind turbines ice distribution and load response under icing conditions. Renewable Energy. **113**, 608–619 (2017)
5. Lamraoui, F.; Fortin, G.; Benoit, R.; Perron, J.; Masson, C.: Atmospheric icing impact on wind turbine production. Cold Reg. Sci. Tech. **100**, 36–49 (2014)
6. Madi, E.; Pope, K.; Huang, M.M.; Lqbal, T.: A review of integrating ice detection and mitigation for wind turbine blades. Renew. Sust. Energ. Rev. **103**, 269–281 (2019)
7. Sabatier, J.; Lanusse, P.; Feytout, B.; Gracia, S.: CRONE control based anti–icing/de–icing system for wind turbine blades. Control Eng. Practice. **56**, 200–209 (2016)
8. Skrimpas, G.A.; Kleani, K.; Mijatovic, N.; Sweeney, C.W.; Jensen, B.B.; Holboell, J.: Detection of icing on wind turbine blades by means of vibration and power curve analysis. Wind Energy. **19**(10), 1819–1832 (2016)
9. Abrahamsson, P.; Eng, M.; Rasmuson, A.: An infield study of road snow properties related to snow–car adhesion and snow smoke. Cold Reg. Sci. Tech. **145**, 32–39 (2018)

10. Cao, Y.H.; Huang, J.S.; Yin, J.: Numerical simulation of three–dimensional ice accretion on an aircraft wing. Int. J. Heat Mass Transf. **92**, 34–54 (2016)
11. Kang, X.; Kang, G.G.; Chang, K.T.; Ge, L.: Chemically stabilized soft clays for road-base construction. J. Mater. Civ. Eng. **27**(7), no04014199 (2015)
12. Tarquini, S.; Antonini, C.; Amirfazli, A.; Marengo, M.; Palacios, J.: Investigation of ice shedding properties of superhydrophobic coatings on helicopter blades. Cold Reg. Sci. Tech. **100**, 50–58 (2014)
13. Wang, Z.J.: Recent progress on ultrasonic de–icing technique used for wind power generation, high–voltage transmission line and aircraft. Energy and Build. **140**, 42–49 (2017)
14. Wang, J.B.; Zhang, J.; Zhang, Y.; Xie, F.; Krajnovic, S.; Gao, G.J.: Impact of bogie cavity shapes and operational environment on snow accumulating on the bogies of high–speed trains. J. Wind Eng. Ind. Aerodyn. **176**, 211–224 (2018)
15. Zhu, Y.C.; Huang, X.B.; Jia, J.Y.; Tian, Y.; Zhao, L.; Zhang, Y.; Cui, Y.T.; Li, X.B.: Experimental study on the thermal conductivity for transmission line icing. Cold Reg. Sci. Tech. **129**, 96–103 (2016)
16. Fakorede, O.; Feger, Z.; Ibrahim, H.; Ilinca, A.; Perron, J.; Masson, C.: Ice protection systems for wind turbines in cold climate characteristics, comparisons and analysis. Renew. Sust. Energ. Rev. **65**, 662–675 (2016)
17. Lv, J.Y.; Song, Y.L.; Jiang, L.; Wang, J.J.: Bio–inspired strategies for anti–icing. ACS Nano. **8**(4), 3152–3169 (2014)
18. Kim, M.S.; Jang, D.U.; Hong, J.S.; Kim, T.: Thermal modeling of railroad with

installed snow melting system. Cold Reg. Sci. Tech. **109**, 18–27 (2015)

19. Zhang, P.; Lv, F.Y.: A review of the recent advances in superhydrophobic surfaces and the emerging energy–related applications. Energy. **82**, 1068–1087 (2015)
20. Cohen, N.; Dotan, A.; Dodiuk, H.; Kenig, S.: Thermomechanical mechanisms of reducing ice adhesion on superhydrophobic surfaces. Langmuir. **32**, 9664–9675 (2016)
21. Koenig, G.G.; Ryerson, C.C.: An investigation of infrared deicing through experimentation. Cold Reg. Sci. Tech. **65**, 79–87 (2011)
22. Parent, O.; Ilinca, A.: Anti–icing and de–icing techniques for wind turbines: Critical review. Cold Reg. Sci. Tech. **65**, 88–96 (2011)
23. Teng, X.; Dong, J.K.; Chen, H.W.; Jiang, Y.Q.; Yao, Y.: Experimental investigation of deicing characteristics using hot air as heat source. Appl. Therm. Eng. **107**, 681–688 (2016)
24. Villalpando, F.; Reggio, M.; Llinca, A.: Prediction of ice accretion and anti–icing heating power on wind turbine blades using standard commercial software. Energy. **114**, 1041–1052 (2016)
25. Villegas, M.; Zhang, Y.X.; Abu Jarad, N.; Soleymani, L.; Didar, T.F.: Liquid–infused surfaces: A review of theory, design, and applications. ACS Nano. **13**, 8517–8536 (2019)
26. Chen, J.; Liu, J.; He, M.; Li, K.Y.; Cui, D.P.; Zhang, Q.L.; Zeng, X.P.; Zhang, Y.F.; Wang, J.J.; Song, Y.L.: Superhydrophobic surface cannot reduce ice adhesion. Appl. Phys. Lett. **101**, no.111603 (2012)

27. Jain, R.; Pitchumani, R.: Facile fabrication of durable copper–based superhydrophobic surfaces via electrodeposition. Langmuir. **34**, 3159–3169 (2018)
28. Nosonovsky, M.; Hejazi, V.: Why superhydrophobic surfaces are not always icephobic. ACS Nano. **6**(10), 8488–8491 (2012)
29. Mahadik, S.A.; Fernando, P.D.; Hegade, N.D.; Wagh, P.B.; Gupta, S.C.: Durability and restoring of superhydrophobic properties in silica–based coatings. J. Colloid Interface Sci. **405**, 262–268 (2013)
30. Oberli, L.; Caruso, D.; Hall, C.; Fabretto, M.; Murphy, P.J.; Evans, D.: Condensation and freezing of droplets on superhydrophobic surfaces. Adv. Colloid Interf. Sci. **210**, 47–57 (2014)
31. Ozbay, S.; Erbil, H.Y.: Ice accretion by spraying supercooled droplets is not dependent on wettability and surface free energy of substrates. Colloid Surf. A-Physicochem. Eng. **504**, 210–218 (2016)
32. Wang, Z.W.; Li, Q.; She, Z.X.; Chen, F.N.; Li, L.Q.: Low–cost and large–scale fabrication method for an environmentally–friendly superhydrophobic coating on magnesium alloy. J. Mater. Chem. **22**, 4097–4105 (2012)
33. Wang, F.J.; Shen, T.H.; Li, C.Q.; Li, W.; Yan, G.L.: Low temperature self–cleaning properties of superhydrophobic surfaces. Appl. Surf. Sci. **317**, 1107–1112 (2014)
34. Zheng, S.L.; Li, C.; Fu, Q.T; Hu, W.; Xiang, T.F.; Wang, Q.; Du, M.P.; Liu, X.C.; Chen, Z.: Development of stable superhydrophobic coatings on aluminum surface for corrosion–resistant, self–cleaning, and anti–icing applications. Materials. Des.

93, 261–270 (2016)

35. Kulinich, S.A.; Farhadi, S.; Nose, K.; Du, X.W.: Superhydrophobic surfaces are they really ice–repellent?. Langmuir. **27**, 25–29 (2011)
36. Farhadi, S.; Farzaneh, M.; Kulinich, S.A.: Anti–icing performance of superhydrophobic surfaces. Appl. Surf. Sci. **257** (14), 6264–6269 (2011)
37. Chen, T.K.; Cong, Q.; Li, Y.; Jin, J.F.; Choy, K.L: Utilizing swelling force to decrease the ice adhesion strength. Cold Reg. Sci. Tech. **148**, 142–127 (2018)
38. Chen, T.K.; Jin, J.F.; Qi, Y.C.; Tian, W.J.; Cong, Q.; Choy, K.L.: Disturbing stability of interface by adopting phase–change temperature gradient to reduce ice adhesion strength. Cold Reg. Sci. Tech. **158**, 69–75 (2019)
39. Jin, Z.Y.; Wang, Y.M.; Yang, Z.G.: An experimental investigation into the effect of synthetic jet on the icing process of a water droplet on a cold surface. Int. J. Heat Mass Transf. **72**, 553–558 (2014)
40. Liu, F.T.; Pan, Q.M.: Facile fabrication of robust ice–phobic polyurethane sponges. Adv. Mater. Interfaces. **2**, no1500219 (2015)
41. McDonald, B.; Patel, P.; Zhao, B.X.: Droplet freezing and ice adhesion strength measurement on super–cooled hydrophobic surfaces. J. Adhes. **93**(5), 375–388 (2017)
42. Tabakova, S.; Feuillebois, F.: On the solidification of a supercooled liquid droplet lying on a surface. J. Colloid Interface Sci. **272**, 225–234 (2004)
43. Xu, Q.; Li, Z.Y.; Wang, J.; Wang, R.F.: Characteristics of single droplet impact on cold plate surfaces. Dry. Technol. **30**, 1756–1762 (2012)

44. Hui, H.; Jin, Z.Y.: An icing physics study by using lifetime–based molecular tagging thermometry technique. Int. J. Multiph. Flow. **36**, 672–681 (2010)
45. Chaudhary, G.; Li, R.: Freezing of water droplets on solid surfaces: an experimental and numerical study. Exp. Therm. Fluid. Sci. **57**, 86–93 (2014)
46. Fumoto, K.; Kawanami, T.: Study on freezing characteristics of supercooled water droplets impacting on solid surface. J. Adhes. Sci. Technol. **26**(4–5), 463–472 (2012)
47. Lazauskas, A.; Guobience, A.; Prosyčevas, I.; Baltrušaitis, V.; Grigaliūnas, V.; Narmontas, P.; Baltrusaitis, J.: Water droplet behavior on superhydrophobic SiO_2 nanocomposite films during icing/deicing cycles. Mater. Charact. **82**, 9–16 (2013)